Structural and spectroscopic properties of Mn-doped $YAlO_3$ ceramics

2008 J. Phys.: Condens. Matter 20 095204

(http://iopscience.iop.org/0953-8984/20/9/095204)

J. Phys.: Condens. Matter **20** (2008) 095204 (8pp) doi:10.1088/0953-8984/20/9/095204

Structural and spectroscopic properties of Mn-doped $YAlO_3$ ceramics

Ya Zhydachevskii[1], A Durygin[2], V Drozd[2], A Suchocki[3,4], D Sugak[5] and J Wrobel[3]

[1] Lviv Polytechnic National University, 12 Bandera, Lviv 79646, Ukraine
[2] CeSMEC, Florida International University, University Park, Miami, FL 33199, USA
[3] Institute of Physics, Polish Academy of Sciences, 32/46 Aleja Lotnikow, Warsaw 02668, Poland
[4] Institute of Physics, University of Bydgoszcz, Weyssenhoffa 11, Bydgoszcz 85072, Poland
[5] Institute of Materials, SRC 'Carat', 202 Stryjska, Lviv 79031, Ukraine

Received 15 November 2007, in final form 10 January 2008
Published 8 February 2008
Online at stacks.iop.org/JPhysCM/20/095204

Abstract

We report results on structural and optical spectroscopic properties of Mn-doped $YAlO_3$ (YAP) ceramics prepared by a solid-state reaction method starting from nanocrystalline oxides. A series of ceramic samples with different Mn concentrations and different Y_2O_3–Al_2O_3 compositions have been studied by means of x-ray powder diffraction, scanning electron microscopy, photoluminescence and thermoluminescence measurements. Peculiarities of YAP phase formation and incorporation of manganese ions into the host are discussed. The possible application of Mn-doped YAP ceramics as thermoluminescent screens for visualization of local heating of various origin, including a heating caused by infrared laser light, has been demonstrated.

1. Introduction

Single crystals of yttrium orthoaluminate with crystal structure of orthorhombic perovskite are known as a host material for solid-state lasers. Manganese-doped yttrium aluminum perovskite (YAP) single crystals became of interest after Loutts *et al* [1, 2] showed their high potential for holographic recording and optical data storage applications. Later, a high thermoluminescence efficiency of the crystals was shown [3], which can be used for thermoluminescent dosimetry of ionizing radiation [4].

From the technological point of view, polycrystalline materials offer significant advantage over single crystals due to the ease and the cost of fabrication. This prompts us to obtain and study Mn-doped YAP ceramics. Note that cerium-doped YAP ($Y_{1-x}Ce_xAlO_3$) prepared by mechanically activated solid-state reaction [5] and complex polymerization methods [6] have already been studied as x-ray scintillators.

This work reports synthesis of polycrystalline Mn-doped YAP samples by the solid-state reaction method as well as results of their characterization by means of x-ray powder diffraction, photo- and thermoluminescence measurements. Optical spectroscopic properties of polycrystalline materials are compared with those of single crystals.

2. Samples preparation and experimental techniques

Polycrystalline Mn-doped YAP samples were prepared by solid-state reaction method starting from nanocrystalline Y_2O_3 (Nanostructured Materials Inc., 99.995%, 29 nm) and Al_2O_3 (Aldrich, nanopowder with particle size <50 nm, γ-phase). Oxide reagents were carefully weighed corresponding to the chemical formulas presented in table 1 and mixed in an agate mortar. Manganese was added during grinding to the mixture of oxides as a solution of $Mn(NO_3)_2$ prepared by dissolution of MnO (Aldrich, 99.99%) in diluted nitric acid. As it is seen from table 1, three series of Mn-doped samples were prepared: (i) with Mn substituting for the yttrium ($Y_{1-x}Mn_xAlO_3$ series), (ii) with Mn substituting for the aluminum ($YAl_{1-x}Mn_xO_3$ series) and (iii) with manganese as a dopant addition to the stoichiometric Y_2O_3–Al_2O_3 mixture ($YAlO_3$:xMn series). After drying, powders were pressed (up to 200 MPa) into pellets and heated at ~1620 K for 5–6 h in air. It should be noted that the chemical formulas presented in the table represent only the chemical composition of the mixture before sintering and hereafter they are used only to identify the samples studied.

The x-ray powder diffraction (XRD) patterns of the studied samples were recorded in the range $2\theta = 10°$–$90°$

Table 1. Phase composition (as derived from GSAS refinement) and orthorhombic crystal lattice parameters of $YAlO_3$ doped with Mn. Standard deviation in crystal lattice parameters determination is 10^{-4} Å or less. (Zero values indicate that the data are below the detection limit. Values in brackets represent a theoretical prediction, assuming that Mn ions occupy Al positions only in the YAP and YAG phases.)

		Phase composition (wt%)			Orthorhombic lattice parameters			
Starting composition	x	$YAlO_3$	$Y_3Al_5O_{12}$	$Y_4Al_2O_9$	a (Å)	b (Å)	c (Å)	V (Å^3)
$YAlO_3$	0	98.4	0.4	1.2	5.1818	5.3294	7.3736	203.62
$Y_{1-x}Mn_xAlO_3$	0.0005	95.5	2.4	2.1	5.1805	5.3295	7.3739	203.59
$Y_{1-x}Mn_xAlO_3$	0.001	91.9	3	5.1	5.1819	5.3303	7.3735	203.66
$Y_{1-x}Mn_xAlO_3$	0.002	95.1	3.5	1.4	5.1804	5.3304	7.3732	203.60
$Y_{1-x}Mn_xAlO_3$	0.005	94.8	3.4	1.8	5.1806	5.3312	7.3721	203.61
		(98.2)	(1.8)	(0)				
$Y_{1-x}Mn_xAlO_3$	0.01	93.8	5.1	1.1	5.1823	5.3334	7.3734	203.80
		(96.4)	(3.6)	(0)				
$Y_{1-x}Mn_xAlO_3$	0.02	88.8	10.2	1	5.1834	5.3356	7.3733	203.92
		(92.7)	(7.3)	(0)				
$Y_{1-x}Mn_xAlO_3$	0.05	77.1	22.9	0	5.1872	5.3469	7.3759	204.57
		(81.5)	(18.5)	(0)				
$YAlO_3$:xMn	0.005	99.4	0.6	0	5.1825	5.3309	7.3740	203.72
$YAlO_3$:xMn	0.02	97.3	2.7	2.7	5.1838	5.3369	7.3742	204.01
$YAl_{1-x}Mn_xO_3$	0.005	97.6	0	2.4	5.1824	5.3312	7.3740	203.73
$YAl_{1-x}Mn_xO_3$	0.02	98.1	0	1.9	5.1831	5.3367	7.3731	203.95

using a Bruker D500 powder diffractometer, operated at 40 kV and 20 mA, with a Cu target tube ($\lambda = 1.5418$ Å).

Angle-dispersive synchrotron x-ray diffraction data were obtained at the microdiffraction beamline of the High Pressure Collaborative Access Team at the Advanced Photon Source by using focused (∼0.01–0.02 mm) monochromatic x-rays ($\lambda = 0.4151$ Å) and a high-resolution image plate detector. The recorded two-dimensional diffraction images (Debye–Scherrer's rings) were integrated with FIT2D [7] and analyzed using the Rietveld method with the GSAS-EXPGUI software package [8, 9]. The starting atomic parameters in the *Pbnm* space group for the $YAlO_3$ were taken from Ross [10] and were used for all refinements.

A Jeol 6400 scanning electron microscope was used to obtain microphotographs of the studied samples.

For the room temperature photoluminescence measurements, a Solar CM2203 spectrofluorimeter was used. A Leybold cryogenerator with LTC60 temperature controller was used for low temperature (10–320 K) measurements. The thermoluminescence measurements in the 300–650 K temperature range were performed using a hand-made setup equipped with a compact furnace and a Triax 320 monochromator with a CCD camera. A linear heating from room temperature up to 650 K with the 0.4 K s^{-1} rate has been used. Application of the monochromator with CCD camera also allowed spectra of emission to be obtained during the thermoluminescence experiments. The monochromator and CCD camera were interfaced by an IEEE 488 (GPIB) to a PC computer where the experimental data were processed and stored. The same monochromator with CCD camera was also used for low-temperature photoluminescence measurements.

Irradiation of samples with γ-rays was performed using a ^{60}Co source with 1.5 kGy h^{-1} dose rate. An Innova 400 Ar^+-laser was used for excitation in photoluminescence and thermoluminescence measurements. A 75 W bulb lamp and 150 W xenon lamp were used for white light excitation.

3. Results and discussion

3.1. Phase and structure analysis of YAP:Mn ceramics

Phase formation in the Y_2O_3–Al_2O_3 system has been studied in detail by many groups for the different kinds of precursor because of the great importance of $Y_3Al_5O_{12}$ garnet (YAG) as a technological material. In addition to the garnet phase, yttrium orthoaluminate $YAlO_3$ and monoclinic $Y_4Al_2O_9$ (YAM) phases exist in this system.

At least two crystal modifications of $YAlO_3$ are known to exist, namely orthorhombic perovskite (YAP) and hexagonal (YAH) polymorph. Furthermore, a third modification, a cubic garnet-type phase, was reported by Yamaguchi *et al* [11]. Of these, the most stable is YAP. The metastable hexagonal phase can be synthesized as a single phase through alkoxide [12] or nitrate evaporation methods [13]. It is usually reported as an intermediate phase accompanying yttrium–aluminum garnet (YAG) synthesis at low temperatures [14, 15].

Synthesis of the pure YAP phase is complicated by the formation of YAM and YAG compositions. The reaction between Y_2O_3 and Al_2O_3 starts by the diffusion of Al^{3+} into Y_2O_3 leading to the yttrium-rich YAM phase crystallizing first [11, 16]. Thus, regardless of the Y_2O_3 and Al_2O_3 starting ratio, the reaction sequence occurring in this system with temperature is as follows:

$$2Y_2O_3 + Al_2O_3 \rightarrow Y_4Al_2O_9 \text{ (1170–1370 K)}$$

$$Y_4Al_2O_9 + Al_2O_3 \rightarrow 4YAlO_3 \text{ (1370–1520 K)}$$

$$3YAlO_3 + Al_2O_3 \rightarrow 4Y_3Al_5O_{12} \text{ (1670–1870 K)}.$$

Moreover, thermodynamic assessment of the Y_2O_3–Al_2O_3 system [17] suggests that YAG + YAM metastable equilibrium is highly possible for the compositional range corresponding to the YAP phase and it can persist even at high temperatures.

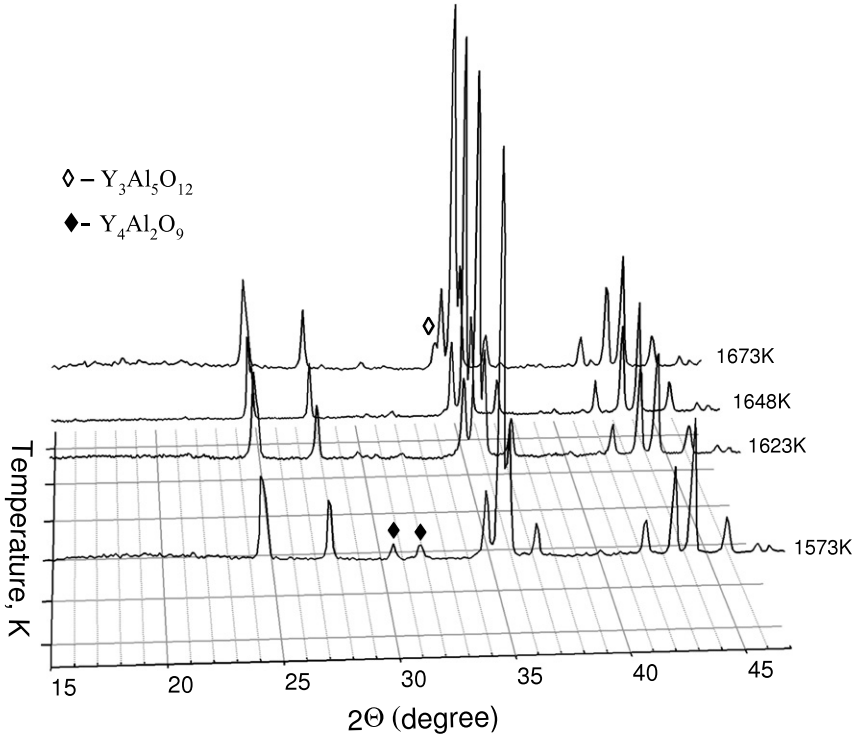

Figure 1. Phase evolution in the Y_2O_3–Al_2O_3 (1:1) system with temperature. The extra peaks corresponding to YAM and YAG phases are marked.

Phase purity of YAP is sensitive to a number of synthesis parameters including the nature of the starting reagents, ratio between them, degree of homogeneity and synthesis temperature. Synthesis of a single-phase YAP was achieved by strict control over the Y:Al ratio (1:1) through heterometal alkoxide $[YAl(OPr^i)_6(Pr^iOH)_2]_2$ molecular precursor [18] or mechanical activation of the Y_2O_3–Al_2O_3 mixture [5].

To study the effect of sintering temperature on the phase purity of YAP, we heated Y_2O_3–Al_2O_3 mixtures (1:1 molar ratio) for 6 h in air at different temperatures. Whereas traces of the YAM phase were observed on XRD patterns of the samples heated at 1570–1620 K, the YAG phase starts to segregate at $T \geqslant 1620$ K (figure 1). In such a way, the temperature of 1620 K was chosen as an optimal one for the synthesis of YAP providing the lowest amount of YAG and YAM impurity phases.

Figure 2 shows the synchrotron x-ray diffraction patterns of the $Y_{1-x}Mn_xAlO_3$ series with different Mn content. YAG and YAM impurity phases were detected on the XRD patterns of all samples. The inset in figure 2 shows the phase composition of the samples as a function of Mn concentration for the $Y_{1-x}Mn_xAlO_3$ series. Weight fraction of YAG in this series gradually increases with increase of Mn doping level reaching almost 23 wt% in the sample with 5 mol% of Mn. On the other hand weight fraction of YAM gradually decreases with increase of Mn content except for sample with $x = 0.001$. Compared to $Y_{1-x}Mn_xAlO_3$, two other series, $YAl_{1-x}Mn_xO_3$ and $YAlO_3$:xMn, contain smaller amount of impurity phases at a certain Mn doping level. Our explanation of this will be done below on the basis of peculiarities of the manganese incorporation into the YAP phase.

The orthorhombic cell parameters obtained after Rietveld refinement for different compositions are reported in table 1. The evolution of the unit cell volume as a function of x values are presented in figure 3. The figure shows a clear linear evolution of the unit cell volume with x for all three series of Mn-doped YAP samples. Our spectroscopic studies presented below indicate that manganese occupies octahedral positions of Al^{3+} ions in YAP structure as Mn^{4+} ions. The ionic radius of Mn^{4+} ions in octahedral coordination (0.53 Å) is very close to that one of Al^{3+} ions (0.535 Å) [19]. Therefore, the incorporation of Mn^{4+} ions into the octahedral positions should not give a large change in lattice parameters. Nevertheless, the unit cell volume of the YAP structure shows a gradually increase with increase of Mn content. Our discussion of possible reasons for this discrepancy will be presented below.

A microstructure of the studied polycrystalline samples is shown in figure 4. A linear dimension of the grains was determined as 0.3 to 0.7 μm.

3.2. Optical spectroscopy of YAP:Mn ceramics

3.2.1. Photoluminescence studies of YAP:Mn ceramics. The photoluminescence measurements using an excitation in the 200–550 nm region revealed a characteristic red emission of the samples shown in figure 5. This emission corresponds to the luminescence of Mn^{4+} ions ($^2E \rightarrow {}^4A_2$ transition) occupying Al positions in YAP [20, 21]. The observed emission spectra of Mn^{4+} ions are identical to those obtained previously for the single-crystalline YAP [21]. Comparing the crystal structure data of YAP [10] with the isostructural $CaMnO_3$ having Mn^{4+} in practically undistorted octahedral

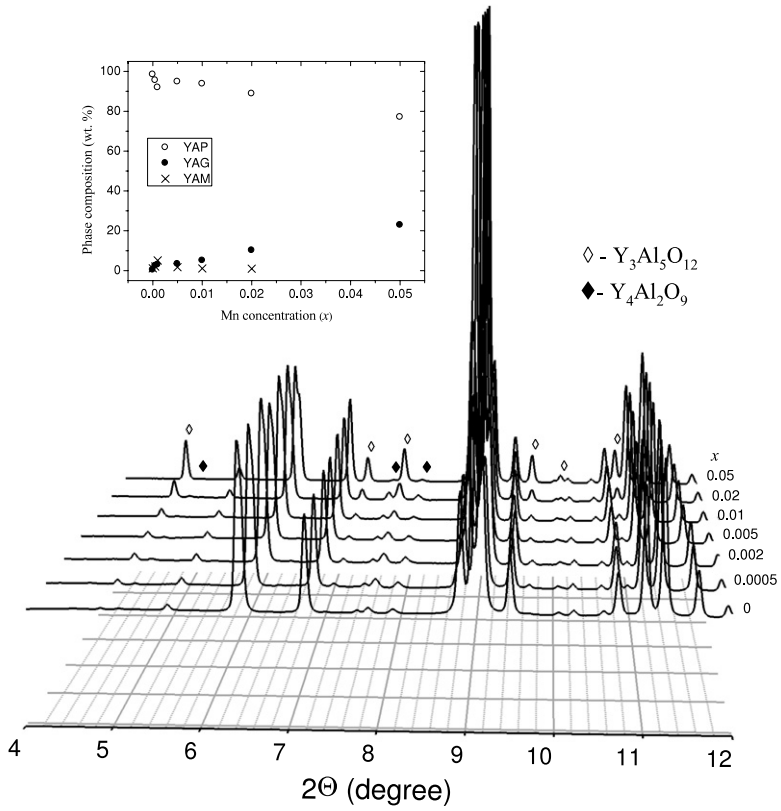

Figure 2. Synchrotron x-ray diffraction patterns of $Y_{1-x}Mn_xAlO_3$ samples with different Mn content (x value) sintered at 1623 K. The extra peaks corresponding to YAM and YAG phases are marked. The inset shows weight fractions of YAP, YAG and YAM phases as functions of x for samples with nominal composition $Y_{1-x}Mn_xAlO_3$.

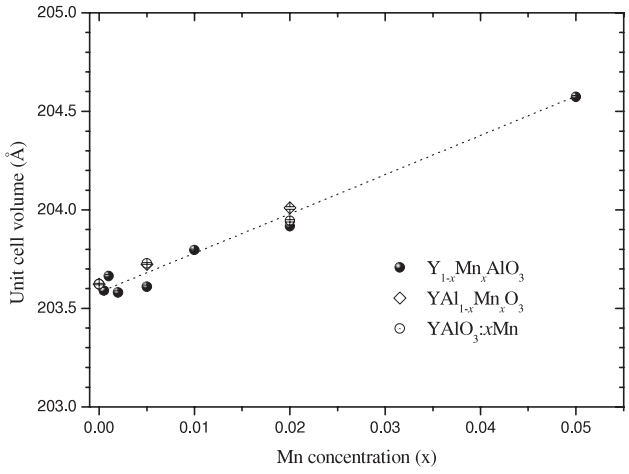

Figure 3. Evolution of the unit cell volume as a function of the Mn concentration for three $YAlO_3$ series studied. The dotted line shown is for eye guide only.

coordination [22], one can suppose that the local structure of Mn^{4+} in YAP is very similar to Al^{3+} in this crystal. The excitation spectrum of the Mn^{4+} luminescence represents a band centered at 485 nm and a much stronger band centered at 325 nm (figure 6). These excitation bands cover all the 200–550 nm spectral range and correlate with absorption bands of Mn^{4+}-doped single crystals reported earlier [1]. The 485 nm excitation (absorption) band corresponds to the $^4A_2 \rightarrow {}^4T_2$ transition in Mn^{4+} ions, while the strong band near 320 nm most likely is the O–Mn^{4+} charge transfer band. In such a way, any wavelength from the 200–550 nm range can be used for optical excitation of Mn^{4+} ions.

Our luminescence measurements using both optical and x-ray excitation did not reveal any other emissions beside Mn^{4+} ions. In such a way we have no evidence of the Mn^{2+} or Mn^{3+} ions in the ceramic samples studied. This allows us to assume that manganese ions in the studied ceramics incorporate only into the aluminum positions in the form of Mn^{4+} ions. The ceramics studied here differ from the single-crystalline YAP:Mn [1–3] where, besides Mn^{4+} in aluminum positions, Mn^{2+} occupying Y positions is also present.

The temperature transformation of the Mn^{4+} luminescence spectrum is shown in figure 7. As YAP:Mn^{4+} single crystals [21], the low-temperature spectra reveal two narrow lines peaked at 691.3 and 692.7 nm (at $T = 10$ K), which correspond to R lines (zero-phonon lines) of the $^2E \rightarrow {}^4A_2$ transition, and the broad structured band in the low-energy side from the R lines corresponds to the vibronic sidebands of the transition. At temperatures above 200 K, the R lines disappear in a growing background of vibronic sidebands and anti-Stokes vibronic sidebands. Relatively small splitting of the ^2E level ($\sim$30 cm^{-1}) observed in YAP testifies also to some distortion of the oxygen octahedra surrounding the Mn^{4+} ions in the crystal.

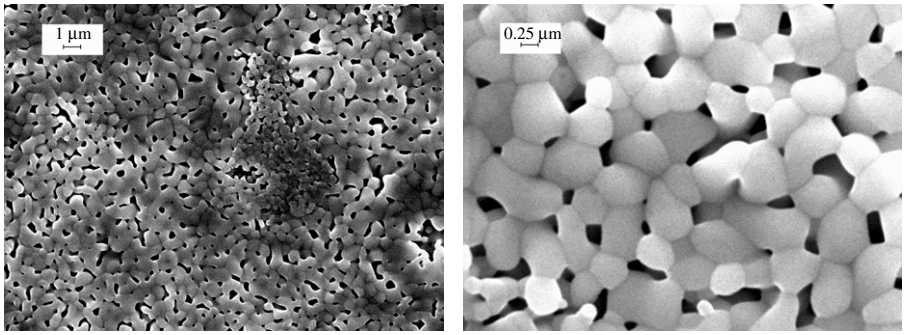

Figure 4. Scanning electron microscope photographs of the $Y_{1-x}Mn_xAlO_3$ ($x = 0.005$) sample obtained at different resolutions.

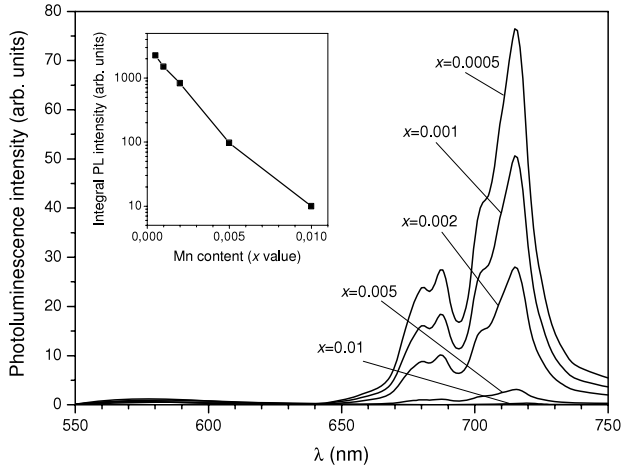

Figure 5. The room temperature emission spectra of Mn^{4+} ions recorded for the $Y_{1-x}Mn_xAlO_3$ samples at $\lambda = 315$ nm excitation. The inset represents the integral intensity of the emission versus Mn content in the samples.

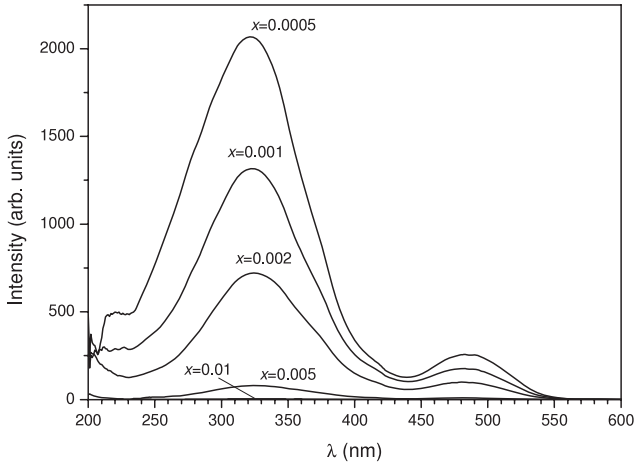

Figure 6. The room temperature excitation spectra of the Mn^{4+} luminescence (registered at $\lambda = 715$ nm) for the $Y_{1-x}Mn_xAlO_3$ samples.

Among all the samples studied, the $Y_{1-x}Mn_xAlO_3$ ($x = 0.0005$) sample has the highest emission intensity. The Mn content in the studied samples is greater and the observed emission intensity of the samples is lower. The emission intensity decrease shows an exponential character (see inset in figure 5). This decrease of the luminescence intensity can be associated with a process of concentration quenching or an excitation energy transfer to the luminescence quenching centers, where concentration increases with Mn content.

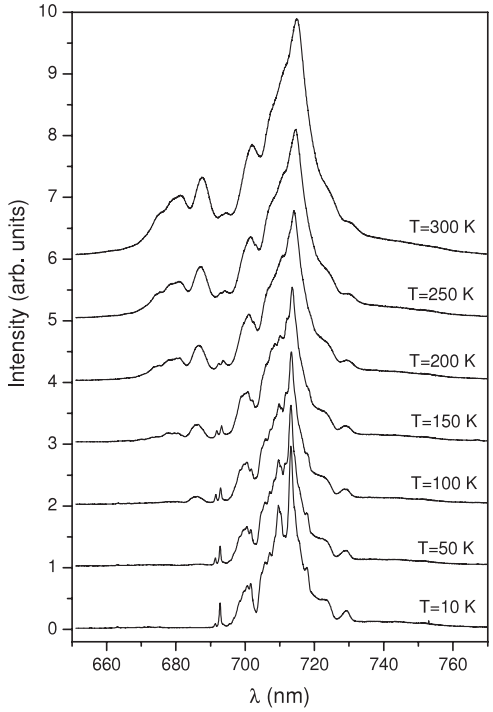

Figure 7. Temperature dependence of the Mn^{4+} luminescence spectra recorded for the $Y_{1-x}Mn_xAlO_3$ ($x = 0.0005$) sample at $\lambda = 488$ nm Ar^+-laser excitation.

Note, that the $YAl_{1-x}Mn_xO_3$ and $YAlO_3$:xMn samples show commensurable emission intensity with the $Y_{1-x}Mn_xAlO_3$ samples at the same nominal content of Mn (x value). Thus, all three samples with the same Mn content of $x = 0.005$ have commensurable emission intensity of Mn^{4+} ions. This allows us to conclude that different ways of doping (at the expense of yttrium or aluminum) do not affect the character of Mn ion incorporation into the YAP structure. In all cases manganese is present in the form of Mn^{4+} ions occupying Al positions and shows the same emission intensity at a certain nominal doping level.

Taking into account that Mn ions occupy Al positions, one can expect a deviation of the ceramics composition from YAP stoichiometry, in particular for the $YAlO_3$:xMn and $Y_{1-x}Mn_xAlO_3$ series, for which the yttrium-deficient composition is formed. The later one gives reasons for the YAG phase formation that indeed is observed experimentally (see table 1).

Assuming that Mn ions occupy only Al positions and knowing a nominal composition of the starting mixture, one can calculate (predict) the phase composition of the ceramics obtained. Assuming that only YAP and YAG phases are formed in this case, we have calculated the phase compositions (the values are presented in table 1 in brackets) for the $Y_{1-x}Mn_xAlO_3$ series ($x = 0.005 \ldots 0.05$) that is strongly yttrium-deficient. Comparing the experimental and theoretically predicted phase compositions for this series one can see some discrepancy between these values. Namely, one observes more YAG phase than is predicted. Moreover, this difference increases with increase of Mn doping level. This discrepancy between the predicted and experimentally observed phase compositions can possibly be associated with the existence of some other impurity phase that contains more yttrium than aluminum and is caused by presence of manganese in the Y_2O_3–Al_2O_3 system. Another possible explanation for this discrepancy is formation of intrinsic defects in YAP and YAG phases that increase the Y/Al ratio. It is known that Y_{Al}^{3+} anti-site defects are common for both YAP and YAG structures [23]. Manganese ions being incorporated into the YAP structure in the form of heterovalent Mn_{Al}^{4+} centers need to be charge compensated and can produce some perturbation stimulating in such a way some intrinsic defect formation. If one supposes that formation of the Y_{Al}^{3+} anti-site defects is somehow related to the Mn_{Al}^{4+} center formation, one can easily associate the observed increase of the unit cell volume of the YAP structure with increasing of Mn content.

3.2.2. Thermoluminescence properties of YAP:Mn ceramics. The samples after exposure to UV or visible light show the characteristic thermal glow during heating above room temperature (figure 8). The thermoluminescence (TL) emission of the studied samples occurs in the red spectral region and corresponds to luminescence of Mn^{4+} ions with spectra identical to ones presented in figure 5. Similarly, as was ascertained for single-crystalline YAP:Mn [2, 24], we assume that optical excitation of Mn^{4+} ions leads to their ionization ($Mn^{4+} \rightarrow Mn^{5+} + e^-$). The resulting electrons are captured on the traps present in the host. During heating of the irradiated samples, the electrons are released from the traps and recombine with Mn^{5+} ions. As a result of such recombination, excited Mn^{4+} ions are created, which relax by way of the characteristic red emission observed in the TL experiments.

However, the thermal glow curves of the studied YAP:Mn ceramics differ from the corresponding ones for the single-crystalline material [25]. The thermal glow for all the studied samples consists of the three peaks at about 330, 420 and 450 K at 0.4 K s^{-1} heating rate in contrast to the three main peaks at 400, 450 and 560 K reported for single-crystalline YAP:Mn under the same experimental conditions. The origin

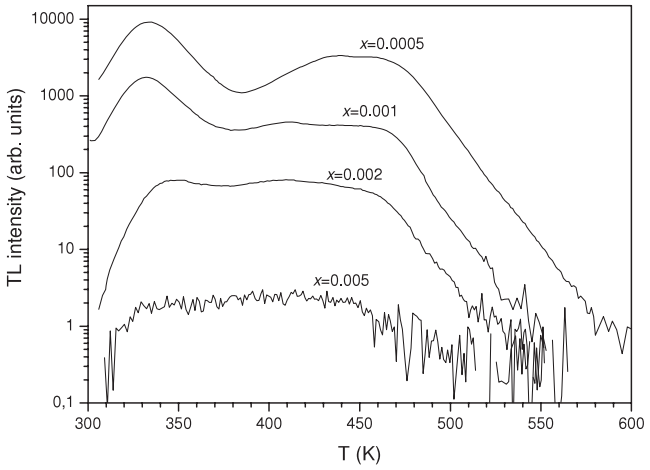

Figure 8. Thermal glow curves recorded for different $Y_{1-x}Mn_xAlO_3$ samples after room temperature excitation with an Ar^+-laser ($\lambda = 488$ nm).

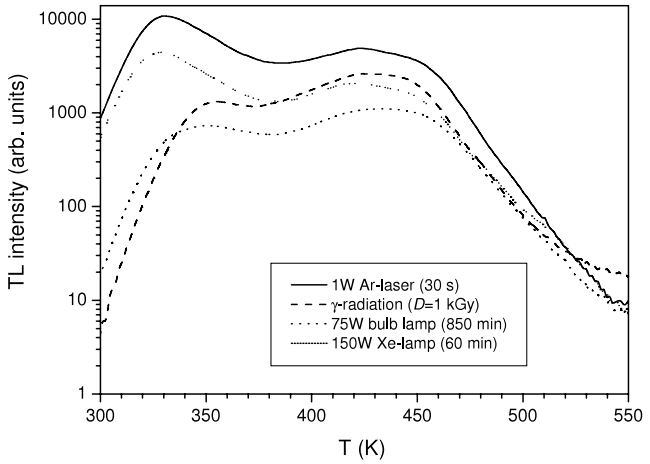

Figure 9. Thermal glow curves recorded for the $Y_{1-x}Mn_xAlO_3$ ($x = 0.0005$) sample after excitation with different types of radiation.

of the electronic traps responsible for the TL peaks observed in single-crystalline YAP:Mn as well as reasons for the difference in the TL peak positions for single-crystalline and ceramic materials are not known and will be the subject of further studies.

As for photoluminescence intensity, the TL intensity of the studied samples decreases with increase of Mn content (see figure 8). Thus the $Y_{1-x}Mn_xAlO_3$ ($x = 0.0005$) sample has the highest TL intensity among the samples studied.

Ionizing irradiation, in particular the γ-radiation used, leads to a similar thermal glow of the samples to that after UV or visible light illumination. The thermal glow after various types of irradiation differs only in the intensity of the glow, which is determined by intensity, irradiation dose and efficiency of the type of radiation used (figure 9). As it is seen from figure 9, a laser light with energy corresponding to the excitation band of Mn^{4+} ions (see figure 6) is one of the most efficient types of radiation, producing the highest thermal glow of the samples. However, a relatively weak source of light

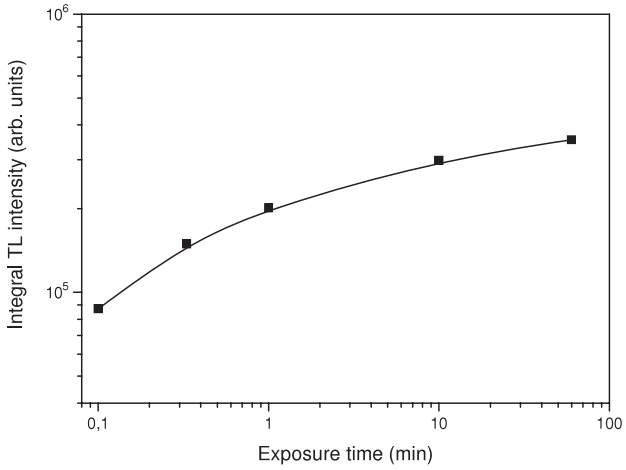

Figure 10. The dose dependence of the integral TL intensity for the $Y_{1-x}Mn_xAlO_3$ ($x = 0.0005$) sample after full-spectrum 150 W Xe-lamp exposition.

such as an ordinary bulb lamp is enough to produce some TL emission, which testifies to the high sensitivity of the material as TL phosphor. The integral TL intensity depending on dose (time) of a 150 W Xe-lamp exposition for example is shown in figure 10.

Owing to the fact that the first TL peak has a maximum slightly above room temperature, a considerable thermal fading of this peak is observed at room temperature. That is why the correlation ratio between the first and the second (third) peaks intensity depends strongly on time passed since irradiation.

The first TL peak situated slightly above room temperature causes a considerable thermal glow of the irradiated sample slightly heated above room temperature. Because of this effect the polycrystalline material studied can be successfully used as a TL screen for the visualization of local heating of various origin, e.g. a heating caused by IR laser light.

The photographs presented in figure 11 demonstrate the performance of the material for visualization of CO_2 laser light. For this purpose the sample was previously irradiated by Ar^+-laser, and after that the sample was tested by a CO_2 laser. The observed thermal glow of the sample (photos (b) and (c) in figure 11) shows a track of the CO_2 laser beam. Thus the studied material can be used as a thermoluminescent alternative to thermographic screens [26, 27], which need to be flooded continuously with UV light. The main advantage of our material over the thermographic screens is that they do not need any illumination during the visualization of the IR laser output. Preliminary exposure of the material to visible or UV light, including sunlight, is enough to obtain the track of the IR laser beam due to the visible TL emission.

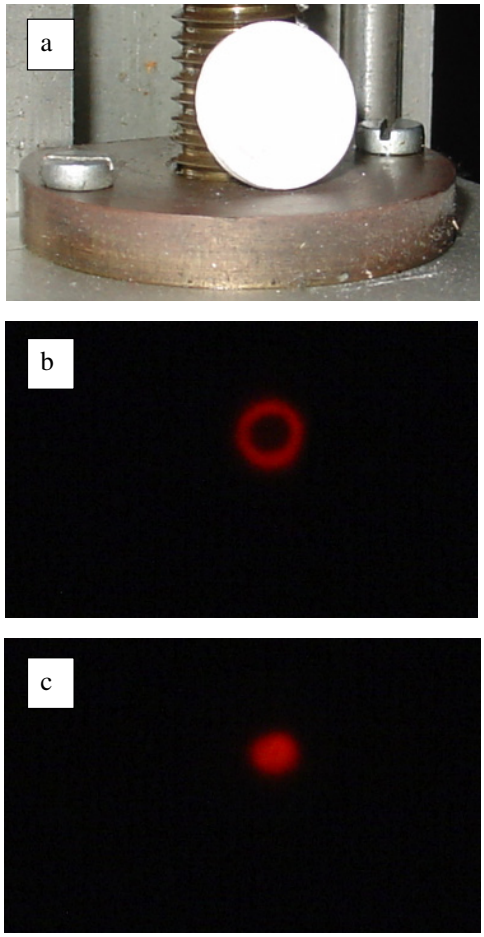

Figure 11. Photographs of the $Y_{1-x}Mn_xAlO_3$ ($x = 0.0005$) sample irradiated for a few seconds by a 1 W Ar^+-laser ($\lambda = 514.5$ nm) (a), and illuminated by 4 W (b) and 2 W (c) power from a CO_2 laser. Photos (b) and (c) were taken in darkness.

(This figure is in colour only in the electronic version)

4. Conclusions

A number of polycrystalline samples of Mn-doped YAP with different Mn concentrations and different Y_2O_3–Al_2O_3 compositions were prepared by solid-state reaction starting from nanocrystalline oxides. The sintering temperature of 1620–1630 K was experimentally chosen as optimal for obtaining YAP ceramics of highest phase purity in the experimental conditions used. Traces of the YAM phase were observed for the samples obtained at lower temperature, whereas traces of the YAG phase dominate at higher temperature.

Scanning electron microscopy of the obtained ceramics samples showed that the grains dimensions ranged from 0.3 to 0.7 μm.

The optical spectroscopy studies testify that different ways of doping (at the expense of yttrium or aluminum) in our sintering conditions do not affect the character of Mn ion incorporation into the YAP structure. In all cases manganese is present in the form of Mn^{4+} ions occupying Al positions and shows the same emission intensity at a certain nominal doping level. The deviation from the YAP stoichiometry caused by the manganese doping, in particular for the $Y_{1-x}Mn_xAlO_3$ series, leads to parasitic YAG phase formation.

The obtained YAP:Mn ceramics demonstrate a high sensitivity to UV or visible light. The samples after exposure show characteristic thermal glow during heating above room temperature. The TL emission occurs in the red spectral region around 710 nm and corresponds to luminescence of Mn^{4+} ions.

The first TL peak situated slightly above room temperature causes a considerable thermal glow of the exposed sample slightly heated above room temperature. Because of this effect the studied ceramics can be successfully used as a TL screen for visualization of local heating of various origins, e.g. a heating caused by IR laser light. Good performance of the material for visualization of CO_2 laser beams has been demonstrated.

Acknowledgments

The authors acknowledge Professor S K Saxena for useful discussion of the experimental results. The work was partially supported by the Ukrainian Ministry of Education and Science (project 'Segnet'), a grant from the National Science Foundation (DMR-0231291), a grant from the Air Force (212600548) and a research grant from the Polish Ministry of Science and Higher Education for the years 2006–2009. Use of the Advanced Photon Source was supported by the US Department of Energy, Office of Science, Office of Basic Energy Sciences, under Contract no. W-31-109-Eng-38.

References

[1] Loutts G B, Warren M, Taylor L, Rakhimov R R, Ries H R, Miller G, Noginov M A, Curley M, Noginova N, Kukhtarev N, Caulfield H J and Venkateswarlu P 1998 *Phys. Rev.* B **57** 3706
[2] Noginov M A, Noginova N, Curley M, Kukhtarev N, Caulfield H J, Venkateswarlu P and Loutts G B 1998 *J. Opt. Soc. Am.* B **15** 1463
[3] Zhydachevskii Ya, Durygin A, Suchocki A, Matkovskii A, Sugak D, Loutts G B and Noginov M A 2004 *J. Lumin.* **109** 39
[4] Zhydachevskii Ya, Durygin A, Suchocki A, Matkovskii A, Sugak D, Bilski P and Warchol S 2005 *Nucl. Instrum. Methods Phys. Res.* B **227** 545
[5] Sakurai K and Guo X 2001 *Mater. Sci. Eng.* A **304–306** 403
[6] Harada M, Ue A, Inoue M, Guo X and Sakurai K 2001 *Scr. Mater.* **44** 2243
[7] Hammersley A P 1997 *ESRF Internal Report* ESRF97HA02T
[8] Larson A C and Von Dreele R B 2004 *Los Alamos National Laboratory Report* LAUR 86
[9] Toby B H 2001 *J. Appl. Crystallogr.* **34** 210
[10] Ross N L 1996 *Phase Transit.* **58** 27
[11] Yamaguchi O, Matui K and Shimuzi K 1985 *Ceram. Int.* **11** 107
[12] Yamaguchi O, Takeoka K and Hayashida A 1991 *J. Mater. Sci. Lett.* **10** 101
[13] Bertaud F E and Mareschal J 1963 *Comptes Rendus* **257** 867
[14] Kinsman K M, McKittrick J, Sluzky E and Hesse K 1994 *J. Am. Ceram. Soc.* **77** 2866
[15] Sim S M, Keller K A and Mah T I 2000 *J. Mater. Sci.* **35** 713
[16] Hay R S 1993 *J. Mater. Res.* **8** 578
[17] Gandhi A S and Levi C G 2005 *J. Mater. Res.* **20** 1017
[18] Mathur S, Shen H, Rapalaviciute R, Kareiva A and Donia N 2004 *J. Mater. Chem.* **14** 3259
[19] Shannon R D 1976 *Acta Crystallogr.* A **32** 751
[20] Noginov M A and Loutts G B 1999 *J. Opt. Soc. Am.* B **16** 3
[21] Zhydachevskii Ya, Galanciak D, Kobyakov S, Berkowski M, Kaminska A, Suchocki A, Zakharko Ya and Durygin A 2006 *J. Phys.: Condens. Matter* **18** 11385
[22] Poeppelmeier K R, Leonowicz M E, Scanlon J C, Longo J M and Yelon W B 1982 *J. Solid State Chem.* **45** 71
[23] Kuklja M M 2000 *J. Phys.: Condens. Matter* **12** 2953
[24] Noginov M A, Loutts G B, Ross K, Grandly T, Noginova N, Lucas B D and Mapp T 2001 *J. Opt. Soc. Am.* B **18** 931
[25] Zhydachevskii Ya, Suchocki A, Sugak D, Luchechko A, Berkowski M, Warchol S and Jakiela R 2006 *J. Phys.: Condens. Matter* **18** 5389
[26] McGee J D and Heilos L J 1967 *IEEE J. Quantum Electron.* **3** 31
[27] Bridges T J and Burkhardt E G 1967 *IEEE J. Quantum Electron.* **3** 168